

Research Article

Evaluation of TiAl₃ Intermetallic Formation Mechanism and Revolution of Annealing Texture in Al/Ti Powder/Al Laminate Composite Fabricated by Cold Roll Bonding and Post-Annealing Treatment

Z. Yazdani*, M.R. Toroghinejad and H. Edris

Department of Materials Engineering, Isfahan University of Technology, 84156-83111, Isfahan, Iran

ARTICLE INFO

Article history:

Received 9 January 2022

Reviewed 29 January 2022

Revised 20 February 2022

Accepted 21 February 2022

Keywords:

EBSD

ODF

Recrystallization

ABSTRACT

In this paper, bulk sheets of multilayer Al-Ti composites were fabricated by cold roll bonding (CRB) at 50% thickness reduction and annealing in different conditions. The effects of annealing temperature and time on the bonding features of Ti-Al have been evaluated. The microstructural changes were studied by scanning electron microscopy (SEM) and focus ion beam microscope (FIB). A field emission electron microscopy (FEG-SEM) equipped with an electron backscatter diffraction (EBSD) tool was utilized to evaluate microstructural and textural changes. This study revealed that CRB composites of Ti-Al can produce the TiAl₃ in relatively short times at annealing temperatures under the Al melting point. The results showed that just the TiAl₃ intermetallic layer formed in the Ti/Al interface by 2 h annealing at 590°C. TiAl₃ formation mechanism can be stated as following stages, Al phase elimination, Kirkendall voids formation, Ti and TiAl₃ phase's volume increasing, micro-crack creation, and finally, easier formation of TiAl₃. Mechanical evaluation of Al/TiAl₃/Al layered composite showed that low ductility is related to growth and joining of Kirkendall voids around Al/TiAl₃ interface that formed after a 2 h annealing at 590°C. Microstructural characterization by EBSD revealed annealing at this condition led to the creation of Al matrix with large grains (about 60 μm) and polycrystalline TiAl₃ intermetallic containing small grains (average 5 μm). One of the main outputs from texture analysis is the recrystallization texture components changing after the formation of the TiAl₃ intermetallic compound. The presence of large Ti aluminide particles resulted into the creation of a new strong P recrystallization texture component besides R5 and Q.

© Shiraz University, Shiraz, Iran, 2022

1. Introduction

Composites combine at least two materials with different physical and chemical properties to present valuable properties [1]. Usually, ductility is often reduced by strength increasing, and advanced industries need materials with both good strength and enough

ductility. Fortunately, composites with a layered structure can enhance the strength with no ductility decreasing and has extended applications in automobile and aerospace engineering [2]. Also, these composites are fabricated by many processes such as explosive cladding [3], hot pressing [4], ultrasonic consolidation [5], and roll bonding [6]. Ti-Al intermetallic compounds

* Corresponding author

E-mail address: z.yazdani@alumni.iut.ac.ir (Z. Yazdani)<https://doi.org/10.22099/IJMF.2022.42741.1212>

represent a high specific strength, high melting temperatures, low density, and good corrosion resistance. Therefore, composites containing these phases can be used as high-temperature structure materials in automobile and aerospace applications [7]. Among Ti-Al intermetallics, TiAl₃ with the density of 3.3 g/cm³ presents the lowest density and also has the highest hardness with the best corrosion resistance [8]. However, their applications are sharply restricted by low ductility. Opportunely, lots of toughening methods have been suggested to boost their ductility, and one of the most successful strategies is the fabrication of composite with Al. Cold roll bonding (CRB) is one of the best solid state methods for the fabrication of composite sheets [9]. There are studies related to the fabrication of Ti-Al intermetallic sheets by CRB and annealing of Ti and Al foils. They tried to eliminate voids with the hot press at the final stage to get a dense composite [10]. There are limited reports about the fabrication of Al/Al layers with Ti powders. In 2011, Wang et al. [11] produced this composite with a good distribution of the TiAl₃ intermetallic phase by depositing molten Al drops onto the Ti powders. there are also some reports about forming this composite in a solid state via accumulative roll bonding and annealing processes [12, 13]. They fabricated a composite with good distribution of TiAl₃ intermetallic compounds in the Al matrix. But the formation mechanism of TiAl₃ intermetallic was not investigated well. In addition, there is no report related to texture and EBSD characterization of this composite. In this study, the Al/TiAl₃/Al layered composite was fabricated by applying CRB after stacking Ti powders and Al sheets, alternately and then annealing them. It is noticeable that the effect of adding Ti powder particles between two Al layers on the bond strength of Al sheets was discussed by these authors [14], and CRB parameters were selected according to previous work. The phase formation and growth actions were studied by more evaluations that were carried out here. For this purpose, a lot of multilayered sheets were produced by differing the annealing process parameters. Additionally, the voids formation mechanism was studied. Besides, interface characterization, mechanical properties, and texture were analyzed and discussed.

2. Experimental Procedure

In this research, annealed Al sheet (1100) with a thickness of 1 mm and Ti powders (0.5 wt.%) were used. Table 1 shows the chemical analysis (wt.%) of used Al. Al sheets were chopped into 100×50×1 mm³ sections and then annealed for 1 h at 350°C. A stainless steel brush was applied on the surfaces of Al sheets to eliminate the oxide layer and create a hard surface.

Table 1. Chemical composition of initial Al (wt.%)

Al	Si	Fe	Cu	Mn	Mg	Cr
99.05	0.156	0.710	0.133	0.047	0.304	<0.015

Preparing initial Ti powders was done by mechanical alloying according to reference [14], to attain small size powders with a small size range. The ball mill process was performed with 5 balls in a planetary ball mill machine (Retsch PM100) in the argon atmosphere for 7 h. The ball to powder weight ratio was selected 10:1, and the speed of the container was 500 rpm. SEM images of Ti powders before and after the ball mill process, are shown in Fig. 1. By milling, the average size of the powder was reduced. The particle size distribution of Ti was determined by the digital image processing (DIP) technique (Fig. 2). After milling, the average size of Ti particles decreases from 45 μm to 0.8 μm.

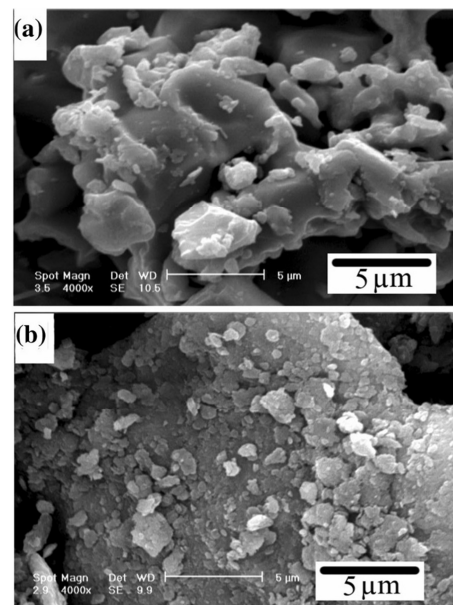


Fig. 1. SEM images of Ti powders (a) before and (b) after ball milling.

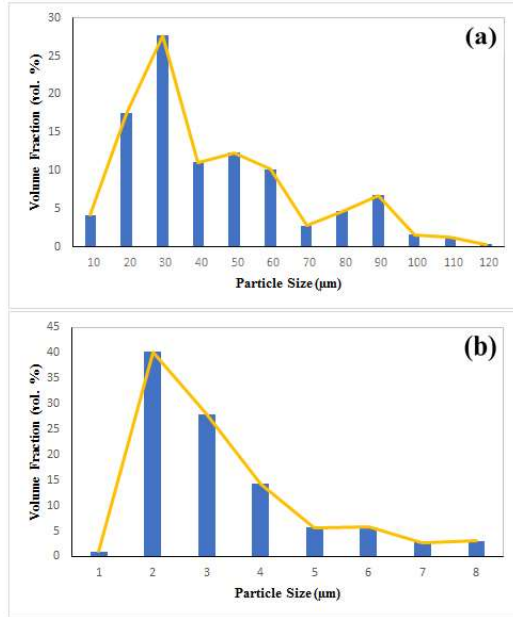


Fig. 2. Image analysis of the Ti particles: (a) before milling, and (b) after milling.

The sandwich of Al sheet/Ti powder/Al sheet was produced by CRB on a laboratory rolling machine using a rolling reduction of 50%. The roll diameter and the rolling speed were 220 mm and 4 m/min, respectively. For the rolled specimens, a series of annealing treatment experiments were performed at 400°C, 500°C, and 600°C at different times.

Microstructure changes evaluations for all specimens were performed by FEG-SEM (Hitachi S-3400) equipped with EDS. A tensile machine (Hounsfield H50ks) was used for tensile evaluations at room temperature with a crosshead speed of 1 mm/min. The total elongation of the specimens was determined as the difference between the gauge lengths before and after testing. Tensile test dimensions were selected according to ASME E 8M and the test was repeated 3 times. A view of the sample preparation for the tensile test is shown in Fig. 3. Another FEG-SEM (LEO 1530FEG) was used for EBSP characterization and micro-texture determination. Focus ion beam analysis was performed by FIB/SEM machine (the Quanta 200 3D Dual Beam).

The thickness of the intermetallic layer versus annealing time in a defined temperature can be exhibited by Eq. (1) [15]:

$$x = kt^n \quad (1)$$

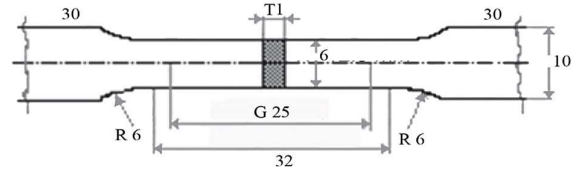


Fig. 3. Schematic of the tensile test sample (all the dimensions are in millimeters).

where x is an average thickness and t is the time of the annealing process, k is the rate constant, and n is the kinetic exponent.

The volume increase of Ti particle after the formation of TiAl_3 intermetallic compound, by ignoring Ti diffusion in Al can be obtained by Eq. (2) [16]:

$$\frac{\Delta V}{V_{\text{Ti}}} = \frac{2.69 \rho_{\text{Ti}} x}{\rho_{\text{TiAl}_3}} - x \quad (2)$$

where $\Delta V/V_{\text{Ti}}$ is Ti volume increase percent, x equals to weight percent of reacted Ti, ρ_{Ti} and ρ_{TiAl_3} are Ti and TiAl_3 density, respectively. The Al matrix hardness and modulus were measured by a nanoindentation instrument (G200). The testing distance, force, and dwell time were 15 μm , 10 mN, and 10 s, respectively. The test was repeated 16 times, and the average value was reported. The hardness values were obtained according to the Oliver-Pharr method [17]. XRD tests were conducted using Philips X'PERTMPD equipment (Amsterdam, Netherlands) with a current of 30 mA and a voltage of 40 kV.

3. Results and Discussion

It must be mentioned that the threshold deformation amount for the Al/0.5 wt.% of Ti powder/Al sheet in this study already earned 45% [12]. According to the results, a 50% thickness reduction, which is greater than the threshold deformation, was selected as the base thickness reduction to continue the research. Fig. 4 represents the SEM image and related EDS of Al/Ti/Al composite after 50% CRB and annealing at 590°C for 2 h. According to this figure, the large Ti particles in this study were converted entirely to the intermetallic phase with TiAl_3 composition determined by EDS analysis. In the Ti and Al diffusion couple, it has been observed that in most cases, the TiAl_3 phase is the first phase to be

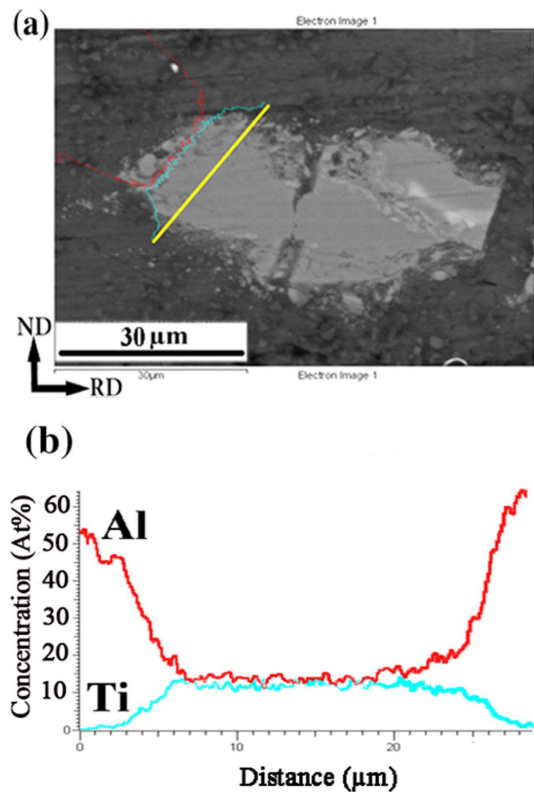


Fig. 4. SEM and EDS image of 50% cold roll bonded sample after annealing treatment at 590°C for 2 h.

formed and is also the phase that is created in large quantities at temperatures under the Al melting point. It is suggested that this is due to an increase in the number of unoccupied spaces in the Al lattice of the $TiAl_3$ layer. They speculated that in the presence of such a gradient, Al diffuses more rapidly, preventing the formation and growth of any expected intermediate phase [18, 19].

Fig. 5 demonstrates the XRD patterns of initial Al, CRB, and CRB-AT samples. It can be observed that after the CRB process, the XRD pattern shows peaks corresponding to only the Al matrix and the added Ti particles, but after the CRB-AT, almost all Ti is turned into the $TiAl_3$ phase. There is a shift of Al peaks towards lower diffraction angles for cold rolled samples and towards higher diffraction angles for heat treated sample. These changes could be due to high dislocation density and internal stresses in the first group, and low lattice size for the second.

Fig. 6 shows the relationship between the thickness of the $TiAl_3$ intermetallic layer and annealing time for different temperatures. The growth rate of the intermetallic

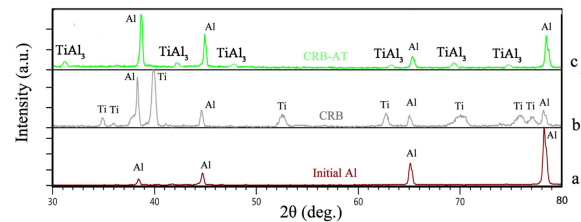


Fig. 5. XRD patterns of (a) initial Al sample, (b) 50% cold roll bonded specimen (CRB), and (c) 50% cold roll bonded specimen after annealing (CRB-AT).

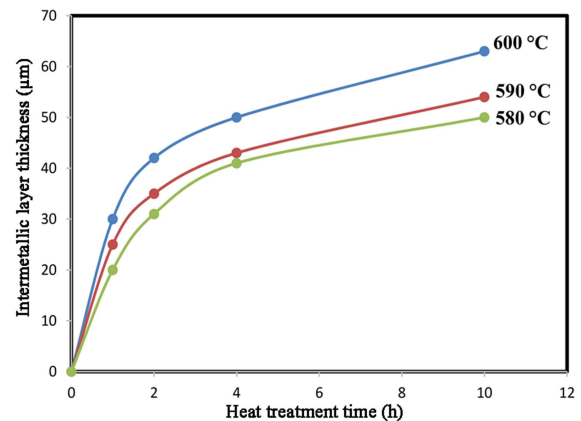


Fig. 6. Changes in the $TiAl_3$ intermetallic layer thickness vs. time at different temperatures for 50% cold roll bonded Al/Ti/Al specimens.

layer increases dramatically by increasing the annealing temperature. The results show that intermetallic growth has a parabolic relationship with time (t). According to Eq. (1), if the chemical reaction controls the process, the amount of n is 1, and if the volume diffusion manages it, the value of n will be 0.5. In this study, the amount of n for the different annealing time range between 1 h and 10 h was estimated as 0.5, which shows that the volume diffusion controls the reaction of $TiAl_3$ intermetallic formation. The growth rate constant k was determined to be equal to $0.21 \mu\text{m}/\text{h}^n$. In the report of Xu et al. [19], it was proved that this process with $n = 0.49$ is managed by the volume diffusion, for annealing times 2 h to 64 h at 550°C. Some previous researchers [20] stated that the $TiAl_3$ intermetallic formation process contains both the chemical reaction and the volume diffusion mechanisms. The first one takes place at the starting times of up to 10 h, and the latter occurred after 10 h. In this study, the occurrence of this mechanism in low time is related to previous CRB that changes microstructure, especially at the interface area. Additionally, Loo et al. [18] stated that

after nucleation of the intermetallic phase during the Ti/Al joint interface, the intermetallic compound layer begins to grow. Diffusion relationships predict that growth has a quadratic relationship with time, usually a function of thickness changes of $t^{1/2}$. Deviation from this behavior can occur when the concentration gradient and diffusion coefficient are not constant. Experiments measuring the growth rate have shown a quadratic relationship between time and thickness in the Ti and Al diffusion system [18]. On the other hand, the presence of oxide layers on the Ti surfaces is the cause of this problem. It has been observed that once the layer diffuses, a normal parabolic growth relationship is established [18].

The results indicate that the diffusion rate between Ti and Al atoms increases with the rise in annealing temperature, which widens the diffusion layer and promotes the formation of the $TiAl_3$ phase. According to previous work of these authors [14], the Ti/Al interfacial bonding strength enhances gradually as the annealing temperature increased from 500 to 600°C.

There is a diffusion bonding with high voids in the interface of the Al matrix and the $TiAl_3$ layer. It was stated that in the Al-Ti system at temperatures below 660°C, the only phase that diffuses is Al [21]. Therefore, some voids establish in previous sites of diffused Al. Examples of these extended voids around $TiAl_3$ intermetallic for cold-rolled Al/Al sandwiches containing Ti powders after 2 h of annealing at 600°C are indicated in Fig. 7. These big voids are created by the joining of voids formed from solitary diffusion Al-Ti couples. These holes are similar to Kirkendall voids, produced in diffusion couples because of the atomic volume difference between Al and $TiAl_3$. On the other hand, according to this figure, intermetallic particle morphology is near rectangular that is similar to particles obtained from friction stir welding in the same system [22]. As the previous report [23] indicates, the Al and Ti solid-state reaction led to the inhomogeneous growth of the $TiAl_3$ layer because of the remaining high amount of Al. Finally, there are a large number of micro-voids located at the interface.

The formation mechanism of $TiAl_3$ intermetallic

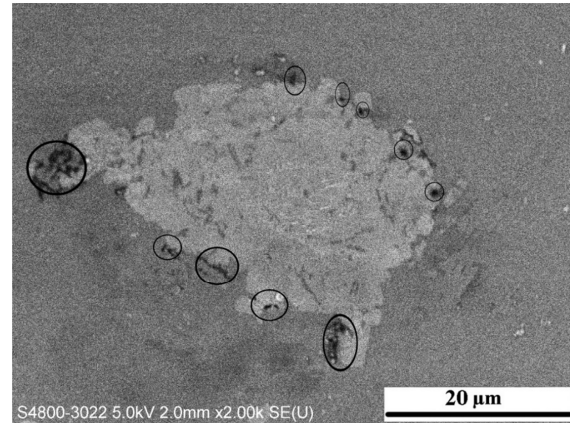


Fig. 7. SEM image of voids around $TiAl_3$ intermetallic for cold roll bonded Al/Ti/Al specimens after annealing at 600°C for 2 h.

compound can be obtained by evaluating the composite microstructure that is reached by annealing at 580°C for the time of 2 h, where the Ti powders consumption has not been yet completed. The microstructure of cold roll bonded Al-Ti-Al specimen after annealing at 580°C for 2 h, prepared by focused ion beam exfoliation, is illustrated in Fig. 8. There are some micro-cracks around the Ti phase. The formation of micro-cracks can relate to the increasing of Ti and $TiAl_3$ phase masses while the intermetallic is fabricated. When Al is present around the Ti particle, that diffusion coefficient of Al in Ti at 590°C is $1.5 \times 10^{-13} \text{ m}^2\text{s}^{-1}$ [24], and the diffusion coefficient of Ti in Al at the same temperature is $3.2 \times 10^{-17} \text{ m}^2\text{s}^{-1}$ [25], Al diffuses in Ti faster than Ti in Al. On the one hand, during diffusion, there is always a high amount of Al, and as a result, an Al-rich $TiAl_3$ intermetallic compound is established. On another hand, by ignoring Ti diffusion in Al, it can be concluded that Al only diffuses to Ti

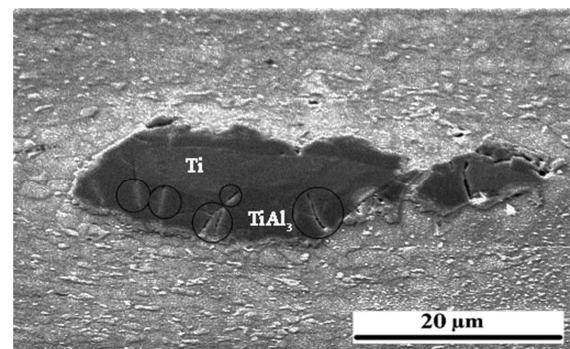


Fig. 8. SEM image of cold roll bonded Al/Ti/Al composite after annealing at 580°C for 2 h.

particle, and vacancies remain at Al because of the Kirkendall effect. Therefore, volume increase occurs at the Ti phase [26]. Additionally, the density of the intermetallic compound is lower than that of Ti, so the formation of this compound also results in a significant increase in volume. Densities of the Ti phase and the $TiAl_3$ compound are 4.5 and 3.4 g/cm³, respectively. Hence, according to Eq. (2), the percent of volume increase is 256%. This result is valid regardless of Ti diffusion in Al. In addition, it is assumed that the whole Ti particle turns to the $TiAl_3$ compound. This volume expansion leads to the formation of tension stress at the outer layer and compression stress at the core of the particle, causing the buildup of micro-cracks during the reaction. Because of these micro-cracks, the reaction of intermetallic compound formation becomes easier and brittle intermetallic blocks simply break into little blocks. These results are consistent with the previous report [27].

According to the results of the present study, the best annealing condition was selected as the temperature of 590°C and time of 2 h. For the purpose of simplicity, in the following, this condition was just referred to as annealing.

Engineering stress-strain curves of initial annealed Al, cold roll bonded Al/Ti/Al under 50% reduction (CRB sample), cold roll bonded Al/Ti/Al after annealing (CRB-AT sample) are presented in Fig. 9. The results show that the ultimate strength and elongation percent of initial annealed Al are 150 MPa and 24%, respectively. After CRB, because of cold work effects, strength is increased to 250 MPa, while elongation is decreased to 9%. Finally, annealing of cold roll bonded specimen led to a reduction of strength, but some parts of elongation recovered by 25% during softening against cold work specimen. According to [28], insufficient bonding in the interface of the Al and the $TiAl_3$ intermetallic layers leads to the spread of premature failure in the intermetallic composite layer, which is more brittle, thus reducing the strength and elongation of the specimen containing the intermetallic phase.

The fracture surfaces of these specimens after the tensile test were examined by SEM and are presented in

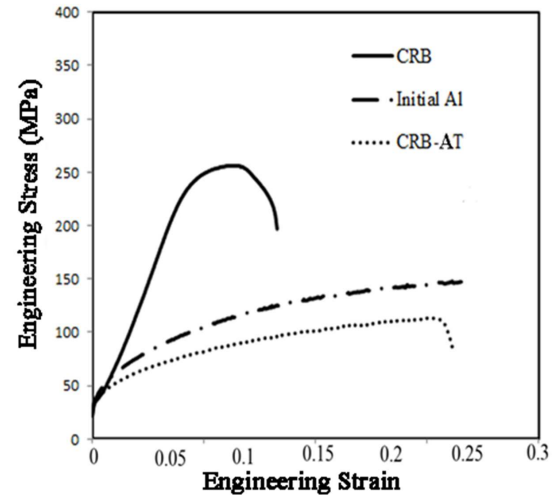


Fig. 9. Engineering stress-strain curves of initial Al, 50% cold roll bonded specimen (CRB), 50% cold roll bonded specimen after annealing (CRB-AT).

Fig. 10. The SEM images of initial annealed Al (Fig. 10(a)), cold roll bonded Al/Ti/Al under 50% reduction (Fig. 10(b)), cold roll bonded Al/Ti/Al after annealing (Figs. 10(c) and 10(d)) are shown as well. According to Fig. 10(a), the fracture surface of the initial annealed Al is indicative of the type of ductile fracture related to the high elongation of Al. For the CRB specimen, there is a high number of dimples or holes at the Al matrix that represents restricted plastic deformation caused by cold work. However, as shown in this figure, the low elongation of this specimen is related to the beginning of rupture between the Al/Ti interface. The fracture surface of cold roll bonded Al/Ti/Al after annealing specimen is exhibited in Fig. 10(c), which indicates the annealing process increases hole's size which means Al matrix has more ductile fracture than cold roll bonded composite. Moreover, $TiAl_3$ intermetallic compounds with high hardness 6 GPa are present at the interface. The internal stress can be increased by the large size of these particles, and in addition, the strength of the Al interface can be declined because of Kirkendall voids. There is a significant rupture at Al/ $TiAl_3$ interface. On another side, the brittle nature of intermetallic particles can lead to early failure. Some researchers stated that Al/Ti composite failure after rolling and annealing is caused due to a fracture in $TiAl_3$ intermetallic compound [29]. According to Fig. 10(d), there are many micron size

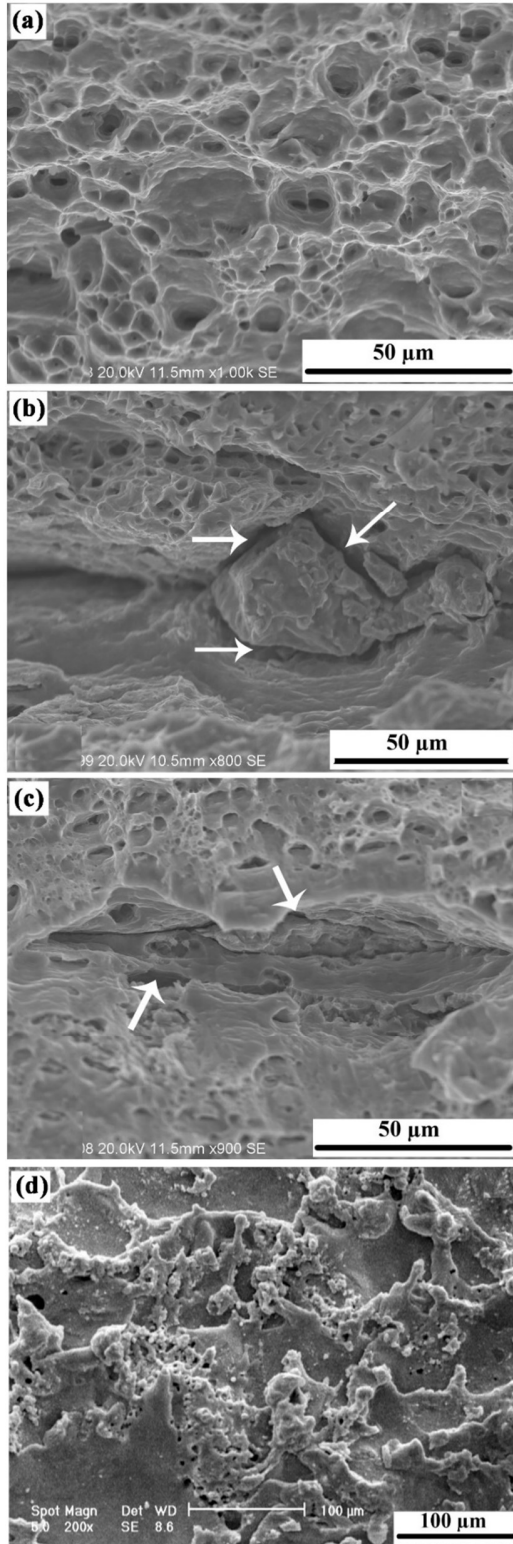


Fig. 10. SEM images of fracture surfaces after tensile test, (a) initial annealed Al, (b) 50% cold roll bonded specimen, (c) 50% cold roll bonded specimen after annealing, and (d) 50% cold roll bonded specimen after annealing at the cross-section of the fracture surface. (Holes and voids are shown with white arrows).

Kirkendall voids up to 10 μm around fractured Al. In comparison with initial Al, fast growth and joining of Kirkendall voids around Al/TiAl₃ interface, which were formed by annealing, led to low ductility of cold roll bonded Al/Ti/Al after annealing specimen.

As the temperature increases in the annealing of the Ti-Al system, the increased bonding strength is beneficial in delaying the early necking and fracture of Al/TiAl₃ composites, thereby enhancing their ductility. The coarsened TiAl₃ phase is easy to induce interface separation. The crack deflection and passivation at the separation can effectively stop the crack propagation, which improves the ductility and formability of Al/TiAl₃ composites surprisingly. The thick and coarse TiAl₃ phases are specifically produced for Al/TiAl₃ composites when annealed at 590°C, but they show excellent elongation. This is attributed to the energy consumption by crack initiation at Ti/Al interface, thus the fracture failure of Ti/Al/Ti composites is postponed [30].

Fig. 11 expresses the results of nanoindentation tests of different specimens. The nano hardness and modulus changes of samples and the related load-displacement curves are revealed in Fig. 11(a) and Fig. 11(b), respectively. According to Fig. 11(a), for the initial Al specimen, the values of nano hardness and modulus are 0.35 and 69 GPa, respectively. After cold roll bonding, the nano hardness and modulus significantly increased and reached up to 0.45 and 150 GPa, respectively. Additionally, this figure proves that after annealing, the high value of nano hardness can be earned, and these parameters are equal to 0.3 and 80 GPa, respectively. According to the Oliver-Pharr method, at a constant maximum load, the higher the maximum displacement after loading, the less the hardness. The initial Al displayed the highest displacement among the tested samples (Fig. 11(b)).

Results of EBSD characterization for CRB Al/Ti/Al composite after annealing are shown in Fig. 12. The electron image of this specimen in Fig. 12(a) indicates that there is a powder particle between Al/Al interface layers. Phase analysis of this particle (Fig. 12(b)) states that the powder particle is related to TiAl₃ intermetallic

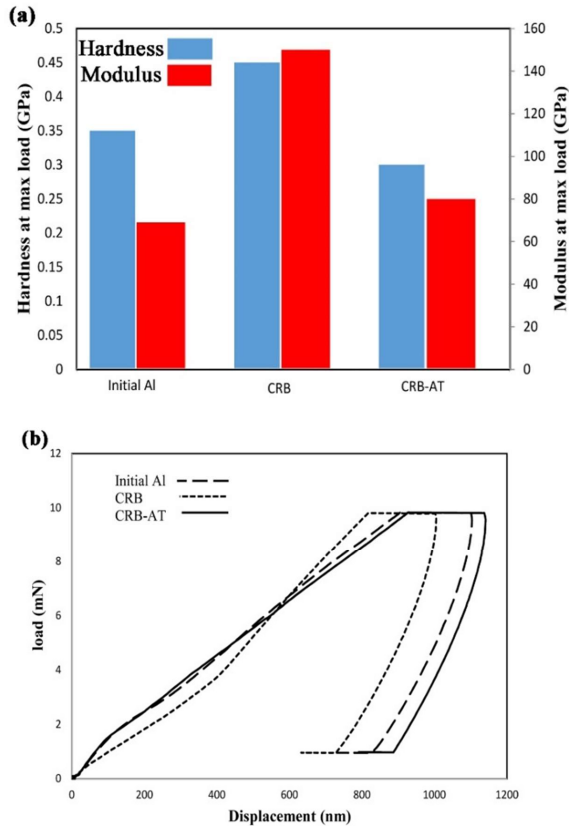


Fig. 11. (a) Nanoindentation hardness, and (b) load-displacement curves of initial Al, cold roll bonded Al/Ti/Al under 50% reduction (CRB), and cold roll bonded Al/Ti/Al after annealing (CRB-AT) specimens.

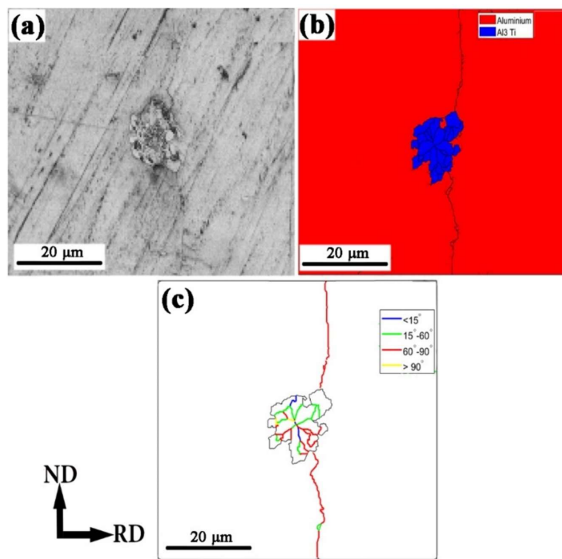


Fig. 12. EBSD evaluation of cold roll bonded Al/Ti/Al after annealing specimen at ND-RD section: (a) electron microscopy image, (b) phase map, and (c) Al matrix boundaries phase.

compound that is represented in the color blue; located in the red Al matrix. Fig. 12(c) indicates the boundaries of the Al matrix with misorientations angles. Main grain boundaries or high angle boundaries contain boundaries with angles bigger than 15, and sub-grain boundaries or low angle boundaries are those with smaller ones. However, tiny low angle boundaries with less than 2° misorientations have not been investigated due to the low accuracy of the electron backscattering measurements [31]. According to this image, the boundaries formed in the Al matrix are the main grain boundaries with misorientations of more than 15° . The grain size of the Al matrix after annealing has grown so much (about 60 μm) that it is, ultimately, not seen in this image and there are a limited number of main grain boundaries between the two Al grains. On the other hand, it is known that the $TiAl_3$ intermetallic phase is a polycrystalline compound containing small grains; the average grain size of which is 5 μm.

The diagram of the misorientations angle distribution obtained from this specimen is also shown in Fig. 13. Fig. 13(a) and Fig. 13(b) show misorientation angle distributions for the Al matrix and $TiAl_3$ intermetallic

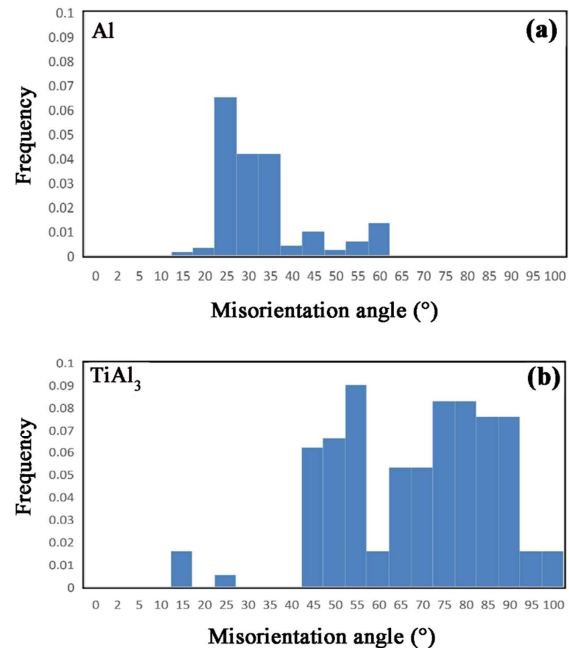


Fig. 13. Misorientation angles distribution for (a) Al matrix, and (b) $TiAl_3$ intermetallic compound of cold roll bonded Al/Ti/Al after annealing specimen.

compounds in this example, respectively. According to these figures, all existing boundaries, belonging to both Al matrix and reinforcement particles, are high-angle boundaries. The maximum intensities for Al and TiAl₃ main grain boundaries are misorientation angles of about 28° and 55°, respectively. For TiAl₃ compound, it may additionally contain a twin-induced peak near 90°.

To investigate the crystal texture, the results of the electron back-scattering test were used. First, Table 2 indicated Miller's indices and Euler's angles for essential texture components in materials with FCC lattice. Important components that are commonly formed by rolling in these materials include Goss, Copper, Brass, Dillamore, Cube, and S. On the other hand, annealing of Al sheets can make significant texture changes including the formation of cubic components, the creation of texture similar to rolling texture, the appearance of one or more components of new texture, and the development of almost random texture [32].

In this study, annealing led to new recrystallization components called P, Q, R, and R5. The recrystallization texture components present in this study, along with Miller's indices and related Euler's angles, are shown in the list of components in Table 2.

Orientation distribution functions (ODF) also provide the ability to analyze texture changes in more detail. These functions can be used to quantify texture in

Table 2. Miller's indices and Euler's angles related to the important components of rolling texture and recrystallization in FCC materials [32]

Texture component	{hkl}	<uvw>	Euler's angles		
			φ_1	Φ	φ_2
Copper, Cu	112	111	90	35	45
S	123	634	59	37	63
Goss, G	011	100	0	45	90
Brass, B	011	211	35	45	90
Dillamore, D	4,4,11	11,11,8	90	27	45
Cubic, Cb	001	100	0	0	0
Rotated Cubic, RCb	001	110	45	0	0
Rotated Goss, RG	110	110	0	90	45
Recrystallization Texture P	011	122	70	45	0
Recrystallization Texture Q	013	231	58	18	0
Recrystallization Texture R	124	211	57	29	63
Recrystallization Texture R5	852	524	65	81	27

terms of a small number of key components. Images obtained from φ_2 sections of 45°, 65°, and 90°, are commonly used to examine the rolling texture, as they contain all the components of FCC deformation texture. The rolling components are shown in Fig. 14.

The pole figures of the (111) plane and the orientation distribution functions at 45°, 65°, and 90° of the φ_2 section, related to the initial Al specimen, cold roll bonded specimen, and the annealed specimen are revealed in Figs. 15 and 16, respectively. It should be noted that the pole figures and orientation distribution functions are measured at half of the sheet thickness. The positions of some important components are shown in (111) pole figures. However, due to the interconnection or proximity of different components in pole figures, it is not possible to determine the exact intensity of the

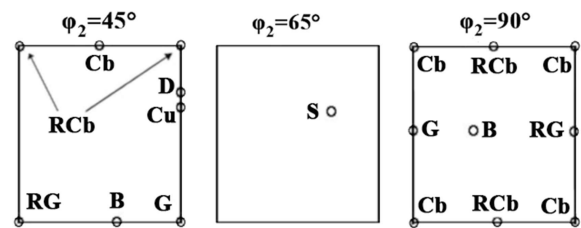


Fig. 14. Schematic of important component positions in rolling materials with FCC structure in φ_2 sections equal to 45°, 65°, and 90°: Brass (B), Copper (Cu), Cubic (Cb), Dillamore (D), Goss (G), Rotated Cube (RCb) and Rotated Goss (RG).

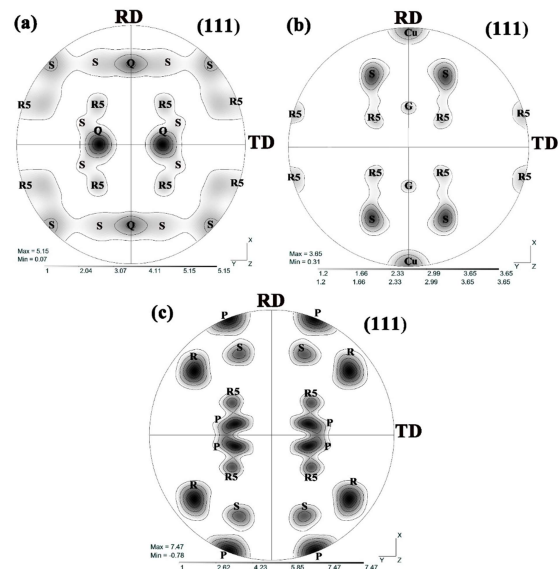


Fig. 15. (111) pole figure of (a) initial Al, (b) cold roll bonded Al/Ti/Al under 50% reduction, and (c) cold roll bonded Al/Ti/Al after annealing specimens.

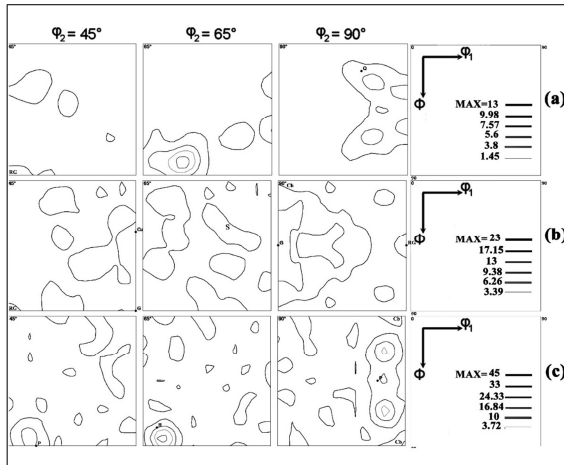


Fig. 16. ODF of (a) initial Al, (b) cold roll bonded Al/Ti/Al under 50% reduction, and (c) cold roll bonded Al/Ti/Al after annealing specimens.

components and to do so, the distribution functions must be used. Fig. 15(a) shows that the initial Al has R5 and Q recrystallization texture components. It also contains the S-rolling texture component, which is associated with the effects of pre-annealing Al deformation. According to Fig. 16(a), the orientation distribution functions for the initial Al specimen confirm the presence of recrystallization texture.

The (111) pole figure of the cold roll bonded (CRB) specimen in Fig. 15(b) indicates the formation of the rolling texture, including the Copper and Goss components. The S component is also strengthened in this case. Among the recrystallization texture components, only the R5 recrystallization component after CRB is present with a slight decrease in intensity. The images of the orientation distribution functions of this specimen, illustrated in Fig. 16(b), indicate the formation of the Goss component, one of the components of the alpha fiber ($\phi_2=90^\circ$).

According to Fig. 15(c), annealing after cold-rolled bonding has led to reinforcing the recrystallization texture component. In this case, in addition to the presence of R5 and R components, another strong component of the recrystallization texture, the P component, has been created. This change in the annealing texture, relative to the initial Al, is associated with large Ti aluminide particles. The presence of the second particle completely changes the movement of the

boundaries, changing the texture of the annealing [32]. The images of the orientation distribution functions for this specimen are also shown in Fig. 16(c) and indicate the disappearance of rolling texture components and the formation of areas with recrystallized texture. On the other hand, the intensity of the fibers decreases due to annealing. Although, the partial appearance of the cube component is also seen here as a result of applying the annealing treatment.

4. Conclusion

1. The cold roll bonding and then annealing at a temperature of 590°C for 2 h led to the creation of the TiAl₃ intermetallic layer.
2. The growth process of the TiAl₃ intermetallic layer is managed by the volume diffusion mechanism. The effect of the temperature on the TiAl₃ intermetallic layer growth is higher than the time of annealing.
3. Formation mechanism of TiAl₃ intermetallic can be described by the following stages: increasing Ti and TiAl₃ phases masses, micro-cracks formation, higher diffusion of Al in Ti, Kirkendall voids remaining in Al, volume increasing at Ti and TiAl₃ phases (256%), stress formation along with particle, micro-cracks establishing and TiAl₃ formation easier accompanying brittle blocks.
4. Evaluation of mechanical properties showed the failure of Al/TiAl₃ composite initiates in the brittle intermetallic layer. This composite also represents hardness and modulus equal to 0.3 and 80 GPa, respectively.
5. According to EBSD characterization, the composite contains the TiAl₃ polycrystalline compound with small grains (5 μm) located in the large grain Al matrix (60 μm).
6. Texture analysis indicated the disappearance of rolling texture components after annealing and the formation of a new recrystallization texture component.

Acknowledgements

The authors gratefully acknowledge Isfahan University of Technology for providing financial support during the research work.

Conflict of Interests

The authors declare that they have no known competing financial interests or personal relationships that could have appeared to influence the work reported in this paper.

5. References

- [1] N. Chawla, K.K. Chawla, Metal matrix composites, Springer, New York, US, 2006.
- [2] Y.J. Wei, Y.Q. Li, L.C. Zhu, Y. Liu, X.Q. Lei, G. Wang, Y.X. Wu, Z.L. Mi, J.B. Liu, H.T. Wang, H.J. Gao, Evading the strength–ductility trade-off dilemma in steel through gradient hierarchical nanotwins, *Nature Communications*, 5 (2014) 3580.
- [3] G.H.S.F.L. Carvalho, I. Galvão, R. Mendes, R.M. Leal, A. Loureiro, Friction stir welding and explosive welding of aluminum/copper: process analysis, *Materials and Manufacturing Processes*, 34(11) (2019) 1243-1250.
- [4] S. Ren, H. Xu, J. Chen, X. Qu, Effects of sintering process on microstructure and properties of flake graphite-diamond/copper composites, *Materials and Manufacturing Processes*, 31(10) (2016) 1377-1383.
- [5] J.S. Seo, H.S. Jang, D.S. Park, Ultrasonic welding of Ni and Cu sheets, *Materials and Manufacturing Processes*, 30(9) (2015) 1069-1073.
- [6] K.K. Yogesha, A. Joshi, N. Kumar, R. Jayaganthan, Effect of cryo groove rolling followed by warm rolling (CGW) on the mechanical properties of 5052 Al alloy, *Materials and Manufacturing Processes*, 32(12) (2017) 1336-1344.
- [7] Y.W. Kim, Intermetallic alloys based on gamma titanium aluminide, *JOM*, 41(7) (1989) 24-30.
- [8] M. Nofar, H.R. Madaah Hosseini, N. Kolagar-Daroonkolaie, Fabrication of high wear resistant Al/Al₃Ti metal matrix composite by in situ hot press method, *Materials & Design*, 30(2) (2009) 280-286.
- [9] D. Pan, K. Gao, J. Yu, Cold roll bonding of bimetallic sheets and strips, *Materials Science and Technology*, 5(9) (1989) 934-939.
- [10] Y.B. Sun, Y.Q. Zhao, D. Zhang, C.Y. Liu, H.Y. Diao, Multilayered Ti-Al intermetallic sheets fabricated by cold rolling and annealing of titanium and aluminum, *Transactions of Nonferrous Metals Society of China*, 21(8) (2011) 1722-1727.
- [11] P.Y. Wang, H.J. Li, L.H. Qi, X.H. Zeng, H.S. Zuo, Synthesis of Al-TiAl₃ compound by reactive deposition of molten Al droplets and Ti powders, *Progress in Natural Science: Materials International*, 21(2) (2011) 153-158.
- [12] Z. Yazdani, M.R. Toroghinejad, H. Edris, A.H.W. Ngan, A novel method for the fabrication of Al-matrix nanocomposites reinforced by mono-dispersed TiAl₃ intermetallic via a three-step process of cold-roll bonding, heat-treatment and accumulative roll bonding, *Journal of Alloys and Compounds*, 747 (2018) 217-226.
- [13] M. Safiri, M. Meratian, M. Panjepor, Fabrication of Al-TiAl₃ composite via in-situ accumulative roll bonding (ARB) and annealing, *Metallurgical and Materials Transactions A*, 50(1) (2019) 415-425.
- [14] Z. Yazdani, M.R. Toroghinejad, H. Edris, A.H.W. Ngan, Effect of cold rolling parameters on bond strength of Ti particle embedded Al strips, *Transactions of the Indian Institute of Metals*, 71(10) (2018) 2497-2504.
- [15] S.B. Jung, Y. Minamino, T. Yamane, S. Saji, Reaction diffusion and formation of Al₃Ni and Al₃Ni₂ phases in the Al-Ni system, *Journal of Materials Science Letters*, 12(21) (1993) 1684-1686.
- [16] D. Roy, S. Ghosh, A. Basumallick, B. Basu, Preparation of Ti-aluminide reinforced in situ aluminium matrix composites by reactive hot pressing, *Journal of Alloys and Compounds*, 436(1-2) (2007) 107-111.
- [17] W.C. Oliver, G.M. Pharr, An improved technique for determining hardness and elastic modulus using load and displacement sensing indentation experiments, *Journal of materials research*, 7(6) (1992) 1564-1583.
- [18] F.J.J. Van Loo, G.D. Rieck, Diffusion in the titanium-aluminum system-II. Interdiffusion in the composition range between 25 and 100 at. % Ti, *Acta Metallurgica*, 21(1) (1973) 73.
- [19] L. Xu, Y.Y. Cui, Y.L. Hao, R. Yang, Growth of intermetallic layer in multi-laminated Ti/Al diffusion couples, *Materials Science and Engineering: A*, 435 (2006) 638-647.
- [20] F. Foadian, M. Soltanieh, M. Adeli, M. Etminkanbakhsh, The formation of TiAl₃ during heat treatment in explosively welded Ti-Al multilayeres, *Iranian Journal of Materials Science and Engineering*, 11(4) (2014) 9-12.
- [21] G.P. Chaudhari, V.L. Acoff, Titanium aluminide sheets made using roll bonding and reaction annealing, *Intermetallics*, 18(4) (2010) 472-478.
- [22] I. Dinaharan, G.A. Kumar, S.J. Vijay, N. Murugan, Development of Al₃Ti and Al₃Zr intermetallic particulate reinforced aluminum alloy AA6061 in situ

- composites using friction stir processing, *Materials & Design*, 63 (2014) 213-222.
- [23] Z.Z. Shen, J.P. Lin, Y.F. Liang, L.Q. Zhang, G.J. Hao, Reaction behaviors occurring in Ti/Al foil metallurgy, *Rare Metals*, 35(1) (2016) 100-105.
- [24] Y. Mishin, C. Herzig, Diffusion in the Ti±Al system, *Acta Materialia*, 48 (2000) 589-623.
- [25] I.C. Barlow, H. Jones, W.M. Rainforth, Evolution of microstructure and hardening, and the role of Al₃Ti coarsening, during extended thermal treatment in mechanically alloyed Al-Ti-O based materials, *Acta Materialia*, 49(7) (2001) 1209-1224.
- [26] Q. Zhang, B.L. Xiao, D. Wang, Z.Y. Ma, Formation mechanism of in situ Al₃Ti in Al matrix during hot pressing and subsequent friction stir processing, *Materials Chemistry and Physics*, 130(3) (2011) 1109-1117.
- [27] V.A. Chianeh, H.M. Hosseini, M. Nofar, Micro structural features and mechanical properties of Al-Al₃Ti composite fabricated by in-situ powder metallurgy route, *Journal of Alloys and Compounds*, 473(1-2) (2009) 127-132.
- [28] C.Y. Liu, R. Jing, Q. Wang, B. Zhang, Y.Z. Jia, M.Z. Ma, R.P. Liu, Fabrication of Al/Al₃Mg₂ composite by vacuum annealing and accumulative roll-bonding process, *Materials Science and Engineering: A*, 558 (2012) 510-516.
- [29] R. Jafari, B. Eghbali, M. Adhami, Influence of annealing on the microstructure and mechanical properties of Ti/Al and Ti/Al/Nb laminated composites, *Materials Chemistry and Physics*, 213 (2018) 313-323.
- [30] M. Cao, C.J. Wang, K.K. Deng, K.B. Nie, W. Liang, Y.C. Wu, Effect of interface on mechanical properties and formability of Ti/Al/Ti laminated composites, *Journal of Materials Research and Technology*, 14 (2021) 1655-1669.
- [31] N. Tsuji, R. Ueji, Y.J. Minamino, Nanoscale crystallographic analysis of ultrafine grained IF steel fabricated by ARB process, *Scripta Materialia*, 47(2) (2002) 69-76.
- [32] F.J. Humphreys, M. Hatherly, Recrystallization and related annealing phenomena, Elsevier, Oxford, 2004.